Accepted for publication in Building and Environment

Overview of three state-of-the-art wind-driven rain assessment models and comparison based on model theory

B. Blocken* [(a)], J. Carmeliet [(b,c)]

(a) Building Physics and Systems, Eindhoven University of Technology, P.O. box 513, 5600 MB Eindhoven, The Netherlands
(b) Chair of Building Physics, Swiss Federal Institute of Technology ETHZ, ETH-Hönggerberg, CH-8093 Zürich, Switzerland
(c) Laboratory for Building Technologies, Swiss Federal Laboratories for Materials Testing and Research, Empa, Überlandstrasse 129, CH-8600 Dübendorf, Switzerland

Abstract
In the past, different calculation models for wind-driven rain (WDR) have been developed and progressively improved. Today, the models that are most advanced and most frequently used are the semi-empirical model in the ISO Standard for WDR (ISO), the semi-empirical model by Straube and Burnett (SB) and the CFD model by Choi, extended by Blocken and Carmeliet. Each of these models is quite different, and to the knowledge of the authors, no comparison of these models has yet been performed. This paper first presents a detailed overview of the three models, including new insights in similarities between these models and relations with recent research results. Based on this overview, it provides a comparison focused on the extent to which the different influencing parameters of WDR are implemented in the models. It shows that the implementation of the influencing parameters is most pronounced for the CFD model, less pronounced for the ISO model and least pronounced for the SB model. It is also shown that in the two semi-empirical models, the values of the wall factor W (for ISO) and the rain admittance function RAF (for SB), which have the same definition in both models, can differ more than a factor 2 from each other. The two models can therefore provide very different results. They also require differently defined reference wind speed values as input. The overview and the comparison in this paper provide the basis for future comparison studies and future improvements of the semi-empirical models.

Keywords: Driving rain; building facade; Computational Fluid Dynamics (CFD); heat, air, moisture transfer (HAM); hygrothermal modelling

1. Introduction

Wind-driven rain (WDR), also referred to as "driving rain", is one of the most important moisture sources for building facades. It is an essential boundary condition for the analysis of the hygrothermal behaviour and durability of historical and contemporary building facade components [1-10]. WDR is governed by a wide range of parameters: building geometry, position on the building facade, environment topography, wind speed, wind direction, horizontal rainfall intensity and raindrop-size distribution. WDR is very complex and characterised by a high spatial and temporal variability. Therefore, assessing the intensity of WDR impinging on building facades is a difficult task. Given its complexity, it is not surprising that, in spite of many decades of intensive research work, WDR is still an active research topic and much work remains to be done.

Three main categories of methods exist for assessing the intensity of WDR on building facades: measurements, semi-empirical models and numerical simulation based on Computational Fluid Dynamics (CFD). The term "semi-empirical" refers to models with a theoretical basis and with coefficients that are – at least partly – determined from measurements. A general review of these three categories of methods can be found in [4]. Measurements are time-consuming, expensive and often impractical. Recent research has revealed that WDR measurements are also very prone to error [11-13]. In addition, measurements made on the facades of a particular building at a particular site, have limited applicability to other facades of other buildings at other sites. This awareness has driven researchers to develop calculation models, which have been progressively improved throughout the years. Today, the models that are most advanced and most frequently used are the semi-empirical model in the ISO Standard for WDR assessment [14] (ISO model), the semi-empirical model by Straube [15] and Straube and Burnett [16] (SB model) and the CFD model by Choi [17-19], extended into the

* **Corresponding author**: Bert Blocken, Building Physics and Systems, Eindhoven University of Technology, P.O.Box 513, 5600 MB Eindhoven, the Netherlands. Tel.: +31 (0)40 247 2138, Fax +31 (0)40 243 8595
E-mail address: b.j.e.blocken@tue.nl

time domain by Blocken and Carmeliet [20,21]. Each of these models is quite different and, to the knowledge of the authors, no comparison of these models has yet been performed.

This paper provides a detailed overview of the three WDR models and a comparison of these models by focusing on their underlying theory and concepts, and the resulting capabilities and limitations. It specifically aims at providing further insights into the model theory, which, for the semi-empirical models, extend considerably beyond the information available in the original documents. New insights in the similarities between models are provided, and several model features are discussed based on recent research results. The overview also supports the comparison study. The overview and comparison study in this paper are intended to support future comparison studies and future improvements of the two semi-empirical models.

The paper contains seven sections. In section 2, the common background of the two semi-empirical models is outlined. In sections 3 to 5, each model is presented and discussed separately. Section 6 compares the models in terms of implementation of the influencing parameters of WDR. The models are also compared in terms of calculation cost and accuracy. Finally, section 7 (summary and conclusions) concludes the paper.

2. Background of the two semi-empirical models

The information presented in this section is for a large part similar to that in [4], but is repeated here because it is essential for the remainder of this paper. Both the ISO and the SB model are based on the WDR relationship, which itself is based on a simple theoretical formula. If we assume that all raindrops are of the same size and that the wind flow is uniform (no increase of wind speed with height), steady and horizontal, the intensity of WDR passing through an imaginary vertical surface can be expressed as [22-24]:

$$R_{wdr} = R_h \cdot \frac{U}{V_t} \tag{1}$$

where R_{wdr} is the WDR intensity through the imaginary vertical surface, R_h is the unobstructed horizontal rainfall intensity (i.e. the intensity of rainfall falling through a horizontal plane, as measured by a standard rain gauge with a horizontal orifice), U is the wind speed and V_t is the raindrop terminal velocity of fall. In this equation, the wind direction is assumed to be perpendicular to the vertical surface at all times. It assumes no deflection of wind or raindrops by the vertical surface and hence is a measure for the "free" or "free-field" WDR. Hoppestad [22] proposed the following formula based on Eq. (1):

$$R_{wdr} = \kappa \cdot U \cdot R_h \tag{2}$$

He called this equation "the WDR relationship" and the factor κ "the WDR coefficient". On-site measured values for κ with free-standing WDR gauges at different locations in Norway ranged from 0.130 to 0.221. Later, Lacy [24,25] refined Eqs. (1-2) by employing the empirical relationships that express the median raindrop size as a function of R_h [26] and the terminal velocity of fall of such raindrops [27], yielding:

$$R_{wdr} = 0.222 \cdot U \cdot R_h^{0.88} \tag{3}$$

where 0.222 (s/m) is the WDR coefficient that results from the adopted empirical relationships. As the empirical expression for median raindrop size represents an average of different measurements, also the value of the WDR coefficient in Eq. (3) should be considered an average value. The exponent 0.88 has often been omitted in WDR research.

Eq. (2) and (3) and the associated WDR coefficients were derived and measured for free-field conditions. The WDR intensity in free-field conditions can be very different from the WDR intensity on a building facade, because of the strongly disturbed wind-flow pattern around the building. To take this effect into account, an adapted WDR coefficient α was introduced in the WDR relationship, as well as a factor $\cos\theta$:

$$R_{wdr} = \alpha \cdot U \cdot R_h^{0.88} \cdot \cos\theta \tag{4}$$

This is the WDR relationship for WDR on buildings. θ is the angle – in a horizontal plane – between the wind direction and the normal to the facade, also called the wind incidence angle. U is a wind speed, which has often not been clearly defined in early WDR research. It can be assumed – but not confirmed – that it is the reference wind speed measured at the standard meteorological height of 10 m. Note that adding $\cos\theta$ implies that only the component of the reference wind velocity vector normal to the facade is considered. This is called the "cosine projection method" [28]. Many researchers measuring WDR on buildings found a very large variation of α with the size of the building and across the building facade: values from 0.02 s/m (9% of 0.222) [24, 29] to 0.26 s/m

(120% of 0.222) [30] have been reported. For the present study, for all three models, the WDR coefficient α will be unambiguously defined as in Eq. (4).

3. The semi-empirical model in the ISO Standard

Before describing and discussing the features of this model, the development history of the ISO Standard for WDR assessment is briefly presented. The reason is the need for clarification amongst the many different standard draft versions that have been developed.

3.1. Development history of wind-driven rain standards

The ISO Standard of 2009, which is the subject of this paper, is the result of a sequence of standards and draft standards, starting from the BSI (British Standards Institution) Draft for Development 93 [31], which was superseded in 1992 by the improved BS 8104 "*Code of practice for assessing exposure of walls to wind-driven rain*" [32]. This code was based on a long series of WDR measurements on buildings at a large number of locations within the UK. Further expansion, based on work by Sanders [1], led to the European Standard Draft PrEN 13013-3 in 1997 [33]. This Standard Draft is closely related to BS 8104, but it replaced the traditional WDR index/WDR map approach to determine WDR exposure [4] by the WDR relationship given in Eq. 4. The main reason for this was that extensive WDR index maps within Europe only existed for the UK. This Standard Draft provided a procedure to analyse hourly weather data (wind speed, wind direction, horizontal rainfall intensity) in order to obtain an estimate of the WDR amount impinging on a building facade or wall of any given orientation ("method1"). The 1997 version of the Draft was extended in 2006 to include a different method ("method2") for those countries in which simultaneous hourly wind and rain measurement data were not available [34]. Method2 is not based on the WDR relationship. Instead it uses 12-hourly averaged wind data and a qualitative recording of the presence and intensity of rain (i.e. the "present weather code" for rain) to calculate the spell length during which masonry is moistened, having a mean return period of 10 years. Note that method2 did not occur in earlier versions of the Standard. It is clearly more limited, less quantitative and therefore inferior to the method based on the WDR relationship, but it was needed to guarantee applicability of the European Standard Draft in all European countries. This version of the Standard Draft has been converted into ISO Standard 15927-3 in 2009: "*Hygrothermal performance of buildings – Calculation and presentation of climatic data – Part 3: Calculation of a driving rain index for vertical surfaces from hourly wind and rain data*." [14]. Only method1 of this Standard will be addressed in this paper.

3.2. Model description

Method1 in the ISO Standard (ISO) provides a procedure to calculate two quantities [14]: (1) the annual average index (as a measure for average WDR exposure) and (2) the spell index (as a measure for maximum or peak WDR exposure). The procedure consists of two steps. First, the airfield index is calculated, which refers to WDR in free-field conditions, i.e. without buildings present, and related to a smooth grass-covered terrain (airfield). Next, this airfield index is converted to a wall index by correction factors to take into account the differences between free-field WDR (as in Eq. 2) and WDR impinging on the building. The correction factors are the roughness coefficient, the topography coefficient, the obstruction factor and the wall factor. Note that the word "index" has been inherited from earlier WDR research; it is used in the ISO Standard to refer to WDR amounts, expressed in L/m² or mm.

3.2.1. Airfield indices

The airfield hourly index is defined as "*the quantity of driving rain that would occur on a vertical wall of given orientation per square meter of wall during 1 h at a height at 10 m above ground level in the middle of an airfield, at the geographical location of the wall*" [14]. The airfield annual index is the airfield index for a given wall orientation totalled over one year. The calculation is performed with at least 10 (and preferably 20 or 30) years of hourly values of wind speed, wind direction and horizontal rainfall intensity from the nearest meteorological station:

$$I_A = \frac{2}{9}\frac{\sum U_{10} \cdot R_h^{8/9} \cdot \cos\theta}{N} \tag{5}$$

where the airfield annual index I_A is expressed in L/m²a (a = annum), U_{10} is the reference wind speed (unobstructed streamwise wind speed at 10 m height) and N is the number of years of available data. The summation is taken over all hours when $\cos\theta$ is positive, i.e. the hours when the wall is windward.

The airfield spell index is defined as the "*airfield index for a given wall orientation totalled over the worst spell likely to occur in any three-year period*". A spell is defined as a period during which WDR occurs, and that is preceded and followed by at least 96 hours with airfield hourly index ($(2/9)U_{10}R_h^{8/9}\cos\theta$) smaller than or equal

to zero. Using at least 10 (and preferably 20 or 30) years of hourly values of wind speed, wind direction and horizontal rainfall intensity, separate airfield indices are calculated for the given wall orientation and for each spell of WDR:

$$I_S' = \frac{2}{9} \sum U_{10} \cdot R_h^{8/9} \cdot \cos\theta \quad (6)$$

where I_S' is expressed in L/m². The summation is again taken over all hours in the spell when cosθ is positive. The airfield spell index I_S is then obtained as the maximum value of I_S' likely to occur once every three years.

3.2.2. Wall indices and correction factors

The wall annual index (I_{WA}) and the wall spell index (I_{WS}) are calculated by multiplying the airfield indices with four correction factors: the roughness coefficient C_R, the topography coefficient C_T, the obstruction factor O and the wall factor W:

$$I_{WA} = I_A \cdot C_R \cdot C_T \cdot O \cdot W \; ; \qquad I_{WS} = I_S \cdot C_R \cdot C_T \cdot O \cdot W \quad (7)$$

The roughness coefficient C_R takes into account the change of mean wind speed at the site due to the height above the ground and the upstream roughness of the terrain. It is given by:

$$C_R(z) = K_R \ln\left(\frac{z}{z_0}\right) \qquad \text{for } z \geq z_{min} \quad (8)$$

$$C_R(z) = C_R(z_{min}) \qquad \text{for } z < z_{min} \quad (9)$$

where z is the height above ground, K_R the terrain factor, z_0 the aerodynamic roughness length and z_{min} a minimum height. Values of K_R, z_0 and z_{min} as a function of the terrain category are given in Table 1. It is noted in the Standard Draft that if a change of upstream roughness occurs within 1 km, the smoothest upstream terrain category must be used. Note that the smoothest terrain category provides the largest C_R value.

The topography coefficient C_T takes into account the increase of mean wind speed over isolated hills and escarpments. It is applied when the wind approaches the slope of the hill or the escarpment and when the building is located at "*more than half way up the slope of a hill" or "within 1.5 times the height of the cliff from the base of a cliff*". It ranges between 1.0 for upstream slopes with less than 5% inclination to a peak value of 1.6 for buildings situated at the crest of steep cliffs or escarpments.

The obstruction factor O takes into account the shelter of the wall by the nearest obstacle, which is at least as high as the wall, along the line of sight from the wall. The line of sight is defined as the "*horizontal view away from the wall, over a sector spanning about 25° either side of the normal to the wall*". The obstruction factor is given in Table 2. It is indicated in the Standard Draft that the obstruction factor may vary significantly at different points along a long wall, and that, if the layout of the built environment is likely to funnel wind towards the wall, the obstruction factor should be taken equal to one, irrespective of the presence of obstructions.

Finally, the wall factor W is defined as the "*ratio of the quantity of water hitting a wall to the quantity passing through an equivalent unobstructed space"*, i.e. the ratio of WDR on the building to free-field WDR. Note that this is not the "airfield" free WDR, but the free-field WDR at the building location, after taking into account the correction factors C_R, C_T and O. The wall factor is a means to account for the type of the wall (height, roof overhang) and the variation of WDR across its surface. The wall factors made available in the ISO Standard are shown in Fig. 1.

3.3. Discussion

The ISO Standard itself does not explicitly use the terms "WDR relationship" and "WDR coefficient". However, combining Eqs. (5-6) and (7), and comparing them with Eq. (4), shows that the ISO model is actually a form of the WDR relationship in which the ratio 2/9 corresponds to Lacy's free-field WDR coefficient 0.222, in which the exponent 8/9 corresponds to Lacy's exponent 0.88, and in which the WDR coefficient is given by:

$$\alpha = \frac{2}{9} \cdot C_R \cdot C_T \cdot O \cdot W \quad (10)$$

Inserting into Eq. (10) into Eq. (4) yields:

$$R_{wdr} = \frac{2}{9} \cdot C_R \cdot C_T \cdot O \cdot W \cdot U_{10} \cdot R_h^{0.88} \cdot \cos\theta \quad (11)$$

Although the Standard strictly only guides the calculation of the average annual amount of WDR and the amount of WDR in the worst likely spell in a three-year period, Eq. (11) could theoretically also be used to determine WDR intensities or amounts for any spell within a year. Note that this is done implicitly within the ISO Standard procedure to determine the annual and spell indices. The ISO model has been used in this way in building physics research to provide boundary conditions for HAM (heat-air-moisture) analysis of building components.

The ISO Standard correctly provides several warnings concerning its applicability and reliability [14], which are mentioned here: (1) The method primarily applies to climates similar to the UK; (2) In all cases, especially in mountainous areas, direct WDR measurements should be made wherever possible; (3) Rain penetration around edges of doors and windows or similar cracks in building facades depends on shorter periods of heavy rain and strong winds; (4) The ISO model is not applicable to mountainous areas with sheer cliffs or deep gorges; (5) It is not applicable in areas where more than 25% of the annual rainfall comes from severe convective storms, i.e. heavy precipitation in the form of showers or thunderstorms generally lasting less than one hour; (6) It is also not applicable in areas and for periods when a significant proportion of precipitation is made up of snow or hail; (7) As to the proximity of meteorological stations, the ISO Standard notes that it will be necessary to decide how representative the values calculated at a meteorological station are for a building at a distant location. Note that the third and fifth warning correspond to the findings by Blocken and Carmeliet [21,35], who indicated that using hourly data, especially for convective rains, can lead to (very) large underestimation errors in the calculated WDR amounts, due to neglecting the sub-hourly co-occurrence of wind and rain. Also note that the Standard does not specify the criteria to determine whether a climate is similar to that of the UK. It also does not provide a quantitative measure for the "significant proportion" of snow or hail in precipitation.

Comparing Eq. (1) with Eqs. (2) and (3) shows that the "free-field" WDR coefficient is theoretically and approximately equal to the inverse of the raindrop terminal velocity of fall. Eq. (3) therefore implies that an average spell could be considered as composed of all similar-sized drops with approximately $V_t = (1/0.222)$ m/s = 4.5 m/s, corresponding to a raindrop diameter of 1.2 mm. This is a realistic value for spells of light to moderate intensity ($R_h \approx 1$ mm/h) [36]. This implies that for other spells (e.g., $R_h < 0.5$ mm/h and $R_h > 5$ mm/h) , this free-field WDR coefficient value might need adjustment, which is not taken into account in the ISO model.

As opposed to many early publications on the WDR relationship, the ISO Standard clearly specifies the wind speed measurement height (10 m) and the reference conditions (airfield).

To determine the wall factor, the ISO Standard only provides the information in Fig. 1. Note that it contains mainly information for low-rise buildings. This is most likely due to the fact that the Standard Draft was written with masonry walls in mind [4], and that it was developed primarily from the UK perspective, and later from the European perspective. The ISO Standard assumes that the wall factors, and therefore the WDR exposure, are the same across the width of the facade, although many WDR measurements in the past have shown that the WDR intensity increases from the middle of the facade to the sides [4]. The Standard provides no comment on this assumption.

While the roughness coefficient C_R is related to the neutral logarithmic mean wind speed profile in the atmospheric boundary layer, the values of the obstruction factor seem to have been chosen quite arbitrarily. Recent CFD simulations have shown that upstream obstructions can also increase, rather than only decrease, WDR exposure [37]. However, we also note that the information in the ISO Standard has been obtained from on-site measurements at the facades of different buildings, that such measurements are difficult and time-consuming, and that the available information has been converted into a quite comprehensive WDR calculation model that takes into account many of the influencing parameters of WDR. In fact, the ISO model is the most comprehensive semi-empirical model known to the authors. In addition, it should be noted that at the time of the introduction of the correction factors, the British Standards Institution [32] explicitly recognized that using these four empirical factors constituted an important simplification of reality, but that this was necessary to avoid complicating the standard too much.

4. The semi-empirical model by Straube and Burnett

4.1. Model description

The model by Straube [15] and Straube and Burnett [16] also starts from Eq. (1), in which they introduce the "Driving Rain Function" DRF as the inverse of the raindrop terminal velocity of fall:

$$R_{wdr} = \frac{1}{V_t} \cdot U \cdot R_h = DRF \cdot U \cdot R_h \quad (12)$$

Note that Straube and Burnett omit the horizontal rainfall intensity exponent 0.88 (see Eq. 3). The DRF is equal to the free-field WDR coefficient as defined in Eq. (2). Straube and Burnett recommend calculating it from the equation by Dingle and Lee [38] for the terminal velocity:

$$V_t(d) = -0.166033 + 4.91844\,d - 0.888016\,d^2 + 0.054888\,d^3 \leq 9.20 \text{ m/s} \quad (13)$$

where d is the raindrop diameter. Concerning the choice of d, they suggest the median diameter from the raindrop spectrum by Best [36]:

$$F(d) = 1 - \exp\left(-\left(\frac{d}{a}\right)^n\right), \qquad a = A R_h^{\,p} \quad (14)$$

where F(d) is the fraction of liquid water in the air with raindrops of diameter less than d, and A, n, p are parameters, the experimentally determined averages of which are 1.30, 2.25 and 0.232, respectively. From Eq. (14), the following equation for the median raindrop diameter can be obtained:

$$\bar{d} = 1.105\, R_h^{\,0.232} \quad (15)$$

Eqs. (12-15) indicate that the DRF or free-field WDR coefficient suggested by Straube and Burnett is a function of raindrop terminal velocity of fall, raindrop-size distribution and horizontal rainfall intensity R_h. This is based on the work by Choi [39], who demonstrated analytically that the DRF is a function of both the raindrop-size distribution and the raindrop terminal velocity of fall, both of which are linked to R_h. Straube and Burnett found that the DRF ranges from 0.20 to 0.25 s/m for average conditions – which corresponds to Lacy's "average" value of 0.222 s/m (see Eq. 3) – but that it varies considerably for different rainfall intensities and rain storm types, from more than 0.5 s/m for drizzle to 0.1 s/m for intense cloudbursts.

The model by Straube and Burnett for WDR on building facades is given by:

$$R_{wdr} = DRF \cdot RAF \,.\, U(z) \cdot R_h \cdot \cos\theta \quad (16)$$

where RAF, the "Rain Admittance Factor", is introduced to convert the free-field WDR intensity to the WDR intensity on the building facade. Based on their own WDR measurements (both free-field WDR and WDR on the walls of a test building) and on a literature review, Straube and Burnett provided values of the RAF in graphical form for three types of building geometries (Fig. 2). They claimed that these contours and values are relatively building-scale independent [16]. The increase of WDR intensity with height is partly taken into account by the presence of the power law function U(z) in Eq. (16), and partly by the RAF values themselves.

4.2. Discussion

The WDR coefficient α has been defined as in Eq. (4). Comparing with Eq. (16) shows that this coefficient in the SB model is given by:

$$\alpha = DRF \,.\, RAF \,.\, \frac{U(z)}{U_{10}} \cdot R_h^{0.12} \quad (17)$$

Taking into account the power-law relationship $U(z) = U_{10}(z/10)^{\beta}$ yields:

$$\alpha = DRF \,.\, RAF \,.\, \left(\frac{z}{10}\right)^{\beta} \cdot R_h^{0.12} \quad (18)$$

where β is the power-law exponent of the mean wind speed profile.

Straube [15] and Straube and Burnett [16] explicitly suggested the use of their model in combination with hourly or 15-minute weather data to provide the WDR boundary condition in HAM models. However, they also provided some specific comments on the reliability of their model. They mentioned that the RAF values were obtained from averaging measurements over several rain events or even years, and that the real RAF during a spell is likely to show a significant variability with wind speed, horizontal rainfall intensity and raindrop-size distribution. They also indicate that the literature contains only a few references to simultaneous measurements of free-field WDR and WDR on buildings. As this is required to determine the RAF, it justifies why the SB model only provides RAF patterns for three types of buildings. Note however that their statement on building-

scale independence of the RAF, given in [16], suggests applicability of these patterns for a wider range of building facade configurations. No specific information on the function U(z) is provided, apart from its power-law distribution.

Finally, note that, in different publications on the SB model [15,16,40], slightly different names are used for the DRF and RAF. The DRF is called "driving rain factor" or "driving rain function", and the RAF is called "rain admittance factor" or "rain admittance function".

5. CFD model

5.1. Background

Starting from 1974, different efforts were made to gain increased insight in the complex interaction between wind, rain and buildings. Sandberg [41] calculated the movements of raindrops around a building based on a flow pattern obtained by wind tunnel modelling. Similar calculations were performed by other authors [42-45]. Souster [46] studied raindrop trajectories based on computed flow patterns around 2D buildings, introducing Computational Fluid Dynamics (CFD) in the area. The break-through for numerical WDR research was the pioneering work of Choi in the first half of the 90ies.

5.2. Model description

The numerical model developed by Choi [17-19] consists of four steps. This model was extended in the time domain by Blocken and Carmeliet [20,21], adding a fifth step. As opposed to the two semi-empirical models outlined in the previous sections, this numerical model has been quite extensively described in the literature. Therefore, only the salient features of the model are described.

The model is based on the definition of two quantities, which have sometimes been given different names by different authors. Here, the names specific catch ratio and catch ratio are used. The specific catch ratio η_d is related to the raindrop diameter d, and the catch ratio η is related to the entire spectrum of raindrop diameters:

$$\eta_d(d) = \frac{R_{wdr}(d)}{R_h(d)}; \quad \eta = \frac{R_{wdr}}{R_h} \tag{19}$$

where $R_{wdr}(d)$ and $R_h(d)$ are the specific WDR intensity on the building and the specific unobstructed horizontal rainfall intensity for raindrops with diameter d. R_{wdr} and R_h respectively refer to the same quantities but integrated over all raindrop diameters. The five steps of the model are:

(1) The wind-flow pattern around the building is calculated using CFD (steady RANS, often combined with a version of the k-ε turbulence model).

(2) Raindrop trajectories are obtained by injecting raindrops of different sizes in the calculated wind-flow pattern and by solving their equations of motion (Lagrangian particle tracking).

(3) The specific catch ratio (η_d) is calculated based on the raindrop trajectories. The calculation is performed for a number of zones on the building facade (e.g. zone A_f in Fig. 3). For each zone, the same procedure is employed. In the steady-state wind-flow pattern – thus neglecting the turbulent dispersion of raindrops – raindrop trajectories of diameter d ending on the corner points of the zone form a "steady" stream tube (Fig. 3). Conservation of mass for the raindrops in the stream tube allows η_d to be expressed in terms of areas:

$$\eta_d(d) = \frac{R_{wdr}(d)}{R_h(d)} = \frac{A_h(d)}{A_f} \tag{20}$$

where A_f is the area of the zone on the building facade where η_d is to be determined and $A_h(d)$ is the area of the horizontal plane bounded by the injection positions of the raindrops of diameter d ending on the corner points of A_f.

(4) The catch ratio (η) is calculated from η_d and from the horizontal raindrop-size distribution. Often, the size distribution by Best [36] is adopted.

(5) When the four previous steps are executed for several combinations of reference wind speed U_{10}, wind direction φ_{10} and horizontal rainfall intensity R_h, the obtained data can be used to construct catch-ratio charts for different zones (positions) at the building facade. Each chart provides the catch ratio η as a function of U_{10} and R_h, for a given position on the building facade and a given φ_{10} (Fig. 4). Experimental data records of U_{10}, φ_{10} and R_h (10-minute values) can then be combined with these catch-ratio charts to determine the corresponding spatial and temporal distribution of WDR on the building facade. Using 10-minute data rather than hourly data has been shown to be very important, especially for convective rain [21,35].

Many applications of the first four steps of the CFD model were performed by Choi [17-19,47,48], Hangan [49], van Mook [12], and others, illustrating the detailed and complex spatial distribution of WDR across various types of building facades. Applications of the five steps of this model for real rain events have been performed by Blocken and Carmeliet [5,20,50,51], Tang and Davidson [52], Abuku et al. [53] and Briggen et al. [54]. As an illustration of a typical result of the 5-step model, Fig. 5 shows contours of the ratio of accumulated WDR to accumulated horizontal rainfall at the end of a rain event, on the south-west facade of a test building with a sloped-roof module and a flat-roof module [51].

5.3. Discussion

Comparing Eq. (19) with Eq. (4) shows that the WDR coefficient in this model is given by:

$$\alpha = \frac{\eta \cdot R_h^{0.12}}{U_{10} \cdot \cos\theta} \tag{21}$$

where η is the catch ratio from CFD simulation(s) with incidence angle θ, corresponding to the wind direction φ_{10}.

The first four steps of the model, listed above, allow determining the spatial distribution of WDR on buildings under steady-state conditions of wind and rain, i.e. for fixed, static values of U_{10}, φ_{10} and R_h. Validation studies of the steady-state simulation technique were performed by e.g. Hangan [49] and van Mook [12]. The extension of this technique in the time domain (fifth step) allows the numerical determination of both the spatial and temporal distribution of WDR on buildings. Validation studies for different buildings and for different rain events have indicated that this extended numerical method can provide quite accurate predictions of the WDR amount and deposition pattern on building facades [5,20,50-54].

Previous studies have clearly shown the power and potential of the CFD model, not only to gain more insight in the interaction between wind, rain and buildings, but also to actually determine the intensity of WDR on building facades. In spite of its large potential, the model also has some specific limitations, as summarized in [4]. These include the need for grid-sensitivity analysis and model validation, the fact that turbulent dispersion is generally neglected and the assumption of a certain raindrop-size distribution.

6. Comparison of the models

6.1. Comparison in terms of implemented influencing parameters

Seven basic parameters can be distinguished that determine the WDR intensity that impinges at a certain position on a building facade: (1) building geometry; (2) position at the building facade; (3) environment topography, (4) wind speed, (5) wind direction, (6) horizontal rainfall intensity and (7) raindrop-size distribution. Environment topography refers to terrain roughness, irregularities such as hills and escarpments, and surrounding buildings and trees. Wind speed refers to both mean wind speed and turbulent fluctuations, and as such includes turbulent dispersion. Table 3 provides a summary of the implementation of each of these parameters in the three models. This is discussed below.

6.1.1. Building geometry and position at the facade

The ISO model only provides information for six typical building facade configurations, and the SB model only for three, although this model also points to building-scale independence of RAF values. In CFD, all types of building configurations can be implemented. Concerning position at the facade; the ISO model provides wall factors W at discrete positions across the facade (Fig. 1) and the SB model provides RAF contours, with minimum and maximum values (Fig. 2). Note that the parameters W and RAF are both defined as the ratio of the WDR intensity on the facade to the free-field WDR intensity, but that they are considerably different at some facade positions (compare Fig. 1 with Fig. 2). For example, at the top edge and the side edges for high-rise buildings, the differences between W and RAF can attain more than a factor 2. In CFD, WDR can be determined at all positions of a facade. The size of A_f (Fig. 3), to be specified by the user, determines the spatial resolution at the facade.

6.1.2. Environment topography and variation of wind speed with height

The ISO model provides correction factors for most features of environment topography, while the SB model can only take into account terrain roughness by the exponent of the power law U(z) in Eq. (16). Therefore, the SB model is strictly only applicable for isolated buildings – or at least buildings with no direct surroundings. All features of terrain topography can theoretically be included in CFD: hills and valleys [55-57], other buildings [37,58] and trees [59,60].

The variation of wind speed with height is taken into account in all three models. In the ISO model, a correction factor (roughness coefficient) is applied for this purpose, which is based on the logarithmic law (Eqs.

8-9). In the SB model, the wind speed in Eq. (16) is a power law expression: $U(z) = U_{10}(z/10)^{\beta}$. In CFD, the variation of wind speed with height is imposed as a boundary condition at the inlet plane, and these inlet profiles should be sustained in the computational domain by appropriate ground-roughness specifications [61-65]. We compare the ISO and SB approach for variation with height. For each ISO terrain category (Table 1), the corresponding power-law exponent β can be determined by fitting the power law to the log law with parameter z_0 from Table 1, at the standard height of 10 m (Fig. 6). This yields: $\beta = 0.125$, 0.16, 0.22 and 0.3 for terrain category I, II, III and IV, respectively. Fig. 7 compares the differences between the ISO and the SB approach for the four terrain categories. Some important observations are made:

(1) Apart from the lowest 4 m, the ISO and SB values are almost identical for terrain category II.
(2) In the ISO model, the overall value of C_R decreases with increasing terrain category, whereas this is opposite for U/U_{10} in the SB model;
(3) In the ISO model, the lower part of C_R is constant, but smaller than one. In the SB model, such feature is not implemented, and the lower part of U/U_{10} goes to zero, implying that the WDR intensity is zero at the bottom of the facade. This however is not the case, as shown by previous studies of WDR [4].

The first two observations can be explained as follows. The reference wind speed U_{10} in the ISO model (Eqs. 5-6, 11) is the wind speed that would occur at 10 m height in the middle of an airfield, at the geographical location of the building: $U_{10,airfield}$. Fig. 7 shows that the correction factor C_R is equal to one at 10 m height for terrain category II, which implies that the airfield situation corresponds to this category. When the building is in reality located on a terrain with higher roughness, the local wind speed $U_{10,real}$ will be lower than the corresponding value $U_{10,airfield}$, and vice versa when the building is located on smoother terrain. This is indicated by the variation of C_R with terrain category in Fig. 7. C_R (Eqs. 8-9) is actually a transformation model for wind speed based on the logarithmic form of the mean wind speed profile. In the SB model on the other hand, no transformation model is implemented. Instead, the implementation of U(z) as power law in Eq. (16) implies that U_{10} is a local reference wind speed, at 10 m height in the same terrain category as the building location. Fig. 7 indeed shows that $U/U_{10} = 1$ in all terrain categories at 10 m height. This means that the SB model in its present form should only be applied with wind speed data corresponding to the terrain category of the building location. Alternatively, the SB model should be extended to include a wind speed transformation model, or such a transformation model should be applied to the transfer/convert the meteorological data to the building site, prior to applying the SB model.

6.1.3. Wind-flow pattern around building and turbulent dispersion

The particular WDR distribution on the building, due to the complex wind-flow pattern around it, is taken into account by W (ISO model) and RAF (SB model), both of which are mainly based on on-site WDR measurements. In CFD, the full interaction between wind and building is included.

Turbulent dispersion of raindrops is not explicitly considered in any of the models. It is implicitly included in the ISO and SB models because W and RAF are based on measurements, in which, to some extent, turbulent dispersion was present. Although CFD can model turbulent dispersion [66], this can not be done with the CFD model based on Lagrangian particle tracking and steady stream tubes (Fig. 3). The reason is that raindrop trajectories influenced by turbulent dispersion are not capable of forming tubes of steady raindrop streams. Based on previous studies in which CFD results were compared with full-scale WDR measurements [20,50,51,53,54], it is expected that the effect of turbulent dispersion is small for low-rise buildings, while it can be quite large for the lower part of high-rise buildings. For a high-rise tower building, CFD simulations of WDR without turbulent dispersion showed good agreement with measurements at the top of the facade, but large underestimations (up to more than a factor 2) for the lower facade parts [54]. This was attributed to neglecting the turbulent dispersion of raindrops. Near the lower part of the facade, the calculated raindrop trajectories are almost parallel to the facade, and do not always intersect with the surface, as shown in [54]. Turbulent dispersion in the streamwise direction can cause these raindrops to deviate from their ‘‘mean’’ trajectory and to hit the facade anyway. For this reason, more rain will hit these lower facade parts when turbulent dispersion is included.

6.1.4. Wind direction, horizontal rainfall intensity and raindrop-size distribution

Wind direction in both the ISO and SB model is taken into account by the cosine projection, while in CFD, simulations with different wind directions can be made. Using the CFD model, Blocken and Carmeliet [28] showed that the cosine projection is strictly not valid, although Janssen et al. [67] indicated that errors averaged over a rain event with the wind direction on average perpendicular to the facade can remain limited.

Horizontal rainfall intensity R_h appears in each of the model equations (Eqs. 5, 6, 11, 16, 19). In addition, it is also included in the SB model when calculating the DRF (Eq. 12-15). A comparison of the influence of R_h between the models can be made by focusing on the expressions for the WDR coefficient α: Eq. 10, 18 and 21. In the ISO model, α is independent of R_h. On the other hand for the SB model, α is a function of $R_h^{0.12}$. The WDR coefficient α varies from 0.58 to 1.74 for values of R_h ranging from 0.01 to 100 mm/h. In the CFD model,

α is a more complex function of R_h, as the catch ratio η itself is a function of R_h, and this function depends on the position at the facade [35].

The horizontal rainfall intensity also influences the raindrop-size distribution. The ISO model does not consider raindrop-size distributions explicitly, although they are implicitly present in the wall factors, which are based on measurements during which different raindrop-size distributions occurred. The SB model takes raindrop-size distributions into account both explicitly (DRF – median diameter) and implicitly (RAF based on measurements). In CFD, any type of raindrop-size distribution can be taken into account in detail. However, since such measurements are generally not available, usually empirical drop-size distribution equations are used, in which R_h is a parameter.

6.2. Comparison in terms of calculation cost and accuracy

Important differences between semi-empirical and CFD models are the calculation cost, in terms of time and storage, and the potential accuracy [4]. The ISO and SB model are easy-to-use and can be applied reasonably quickly, at the expense of lower resolution and generally lower accuracy. CFD simulations of WDR based on Lagrangian particle tracking are time-consuming, because raindrop trajectories for each raindrop diameter d have to be calculated in wind-flow patterns with different reference wind speeds and wind directions. On the other hand, it is clear that CFD can provide much more detailed information as illustrated, for example, by comparing the information provided in Figs. 1, 2 and 5,. If CFD is carefully applied, results from validation studies have shown that such information can be in good agreement with experimental data [20,50-54].

Although the steady stream-tube model (CFD-ST) will be less accurate than a model that includes turbulent dispersion in a proper way (CFD-TD), the former is generally preferred over the latter. One of the main reasons is calculation cost. Application of the CFD-ST model is already very time-consuming. With this model, calculating the specific catch ratio for a certain drop diameter and at a certain facade position requires calculating only three raindrop trajectories that form a stream tube ending near this facade position. However, as steady stream tubes do not exist when turbulent dispersion is included (CFD-TD model), the specific catch ratio in such case should be determined by releasing a large number of drops, and counting the number of drops that impinge at a certain facade position. The specific catch ratio is then the ratio of the number of impinged drops (at that position) versus the number of injected drops from a certain reference position. For every facade position, many raindrop trajectories are needed to achieve results that are independent of the injection positions and the number of injections, which are chosen by the user. In short, the sophistication and efficiency of the CFD-ST model is lost when turbulent dispersion is included. In addition, accurately modelling turbulent dispersion requires accurate information on the turbulence field. Given the deficiencies of the k-ε family of turbulence models, second moment closure but possibly LES (Large Eddy Simulation) or hybrid LES/URANS (Unsteady RANS) will be required. Resorting to such transient wind-flow pattern calculations will drastically increase computation times.

The Lagrangian approach is the natural approach for dealing with particle motion. In this approach, individual particles are tracked as they move through the computational domain. This approach is sometimes also referred to as the non-continuum approach, because particle phase is dealt with in a discrete way. As an alternative to the Lagrangian approach, the Eulerian approach can be considered [68,69,70]. In this approach, the particle phase is treated as a continuum, and its characteristics are obtained by solving the partial differential equations for particle continuity and particle momentum in a given coordinate system. This approach is also referred to as the continuum or two-fluid approach [69]. Often, a Boussinesq approximation is used to relate the turbulent particle flux to the average particle concentration gradients in the particle phase equations. Loth [68], Shirolkar et al. [69] and Zhang and Chen [70] describe advantages and disadvantages of both approaches. Some of these are briefly mentioned below, from the viewpoint of WDR modelling. Some of the main advantages of the Lagrangian approach are that it generally does not rely on gradient diffusion approximations, and it can elegantly take into account inertia effects, crossing trajectory effects and temporal and cross-correlations in the turbulence velocity [69]. A disadvantage is the difficulty in estimating the appropriate time and length scale of the turbulence [69]. Lagrangian modelling for WDR will generally also be significantly more time-consuming than Eulerian modelling. Advantages of the Eulerian approach are that the particle phase can be treated with the same discretisation and numerical techniques as the continuum (fluid) phase. This is beneficial for including two-way coupling effects. It can also strongly reduce the computational cost. Disadvantages can be the gradient diffusion approximation and numerical diffusion [68,69]. To the knowledge of the authors, Eulerian modelling has not yet been applied for WDR.

7. Summary and conclusions

This paper has presented a detailed overview of three calculation models for wind-driven rain (WDR) on buildings and a comparison of these models based on model theory. These models are the semi-empirical model in the ISO Standard (ISO model), the semi-empirical model by Straube and Burnett (SB model) and the CFD

model by Choi, extended by Blocken and Carmeliet (CFD model). First, the historical and theoretical background, as well as the capabilities and limitations of each model have been described. Next, the models have been compared in terms of how the influencing parameters of WDR are implemented, and in terms of calculation cost and accuracy. The following conclusions are made:

(1) Although they are both based on the WDR relationship, the ISO model and SB model are quite different:
   a. The ISO model uses a constant free-field WDR coefficient (0.222 s/m), whereas in the SB model the DRF is a strong function of horizontal rainfall intensity R_h, which is closer to reality.
   b. The ISO model includes a transformation model to convert the wind speed at a standard meteorological station (airfield) to the building site. The SB model lacks such a transformation model. The reference wind speed U_{10} in the ISO model corresponds to terrain category II (airfield), while U_{10} in the SB model corresponds to the local terrain roughness (i.e. at the location of the building). This means that not just any meteorological data can be used as input to each of these models, and appropriate conversions need to be made.
   c. The ISO model provides correction factors to take into account the effect of topographic features such as hills and valleys, and surrounding obstacles such as buildings and trees. The SB model does not provide such factors.
   d. The ISO wall factor W and the SB rain admittance function RAF have the same definition, but their values in both models are considerably different for some facade positions. For example, at the top edge and the side edges for high-rise buildings, the differences between W and RAF can be more than a factor 2. The two models can therefore provide very different results.
   e. The ISO model provides a single result, while the SB model provides a minimum and maximum limit for the WDR intensity, resulting from the minimum and maximum limit for the RAF.
   f. In the ISO model, the WDR coefficient α is independent of R_h, while in the SB model it is a function of $R_h^{0.12}$.

(2) The CFD model inherently exhibits a considerably stronger implementation of the influencing parameters of WDR on buildings than the two semi-empirical models, and is therefore potentially more accurate, at the expense of increased model complexity and calculation cost. The ISO model is the most comprehensive semi-empirical model known to the authors; it provides a more pronounced implementation of the influencing parameters than the SB model.

(3) The CFD model is too complex and too costly for widespread practical use. It can however be used to evaluate the two semi-empirical models and to improve their performance.

(4) It should be noted that the two semi-empirical models are without any doubt considered very valuable. These models provide a strong and necessary basis for further model development, which can be guided by – among others – validated CFD simulations.

(5) The detailed overview and the comparison in this paper provide the basis for future comparison studies. and for future improvements of the two semi-empirical models. The future comparison studies will include application of the three calculation models to calculate WDR for a range of idealized and real building configurations.

Acknowledgements

The authors are grateful to the European Committee for Standardization (CEN) for the permission to reproduce Fig. 1.

Notation

A_f	area of a zone on the building facade (m²)
A_h	area of a horizontal surface at a certain height in the upstream undisturbed flow (m²)
a	annum (per annum = per year)
a, A, n, p	parameters in raindrop-size distribution equation
C_R	roughness coefficient
C_T	topography coefficient
d	raindrop diameter (mm)
$\bar{d}$	median raindrop diameter (mm)
$f_h(d)$	probability-density function of raindrop size falling through a horizontal plane (m^{-1})
I_A	airfield annual index (L/m²a)
I_S	airfield spell index (L/m²)
I'_S	airfield index for a given spell (L/m²)
I_{WA}	wall annual index (L/m²a)
I_{WS}	wall spell index (L/m²)
K_R	terrain factor
N	number of years of available data

O	obstruction factor
R_h	horizontal rainfall intensity, i.e. through a horizontal plane (L/m²h or mm/h)
R_{wdr}	wind-driven rain intensity (L/m²h or mm/h)
S_h	horizontal rainfall amount, i.e. through a horizontal plane (L/m² or mm)
S_{wdr}	wind-driven rain amount (L/m² or mm)
U	streamwise horizontal component of the mean wind-velocity vector (m/s)
U_{10}	reference wind speed at 10 m height in the upstream undisturbed flow (m/s)
V_t	raindrop terminal velocity of fall (m/s)
W	wall factor
z	height above ground (m)
z_0	aerodynamic roughness length (m)
z_{min}	minimum height (m)
α	wind-driven rain coefficient
β	power-law exponent of mean wind speed profile
ε	turbulence dissipation rate (m²/s³)
η_d	specific catch ratio
η	catch ratio
θ	angle between the wind direction and the normal to the facade/wall (° from north)
κ	free-field wind-driven rain coefficient
φ_{10}	wind direction at 10 m height in the upstream undisturbed flow (degrees from north)
BSI	British Standards Institution
CEN	European Committee for Standardisation
CFD	Computational Fluid Dynamics
DRF	Driving Rain Function
ISO	International Organization for Standardization
RAF	Rain Admittance Factor
RANS	Reynolds-Averaged Navier-Stokes
SB	Straube and Burnett
VLIET	Flemish Impulse Programme for Energy Technology
WDR	Wind-Driven Rain

References

[1] Sanders C. Heat, air and moisture transfer in insulated envelope parts: Environmental conditions. International Energy Agency, Annex 24. Final report, volume 2. Acco, Leuven, 1996.

[2] Dalgliesh WA, Surry D. BLWT, CFD and HAM modelling vs. the real world: Bridging the gaps with full-scale measurements. Journal of Wind Engineering and Industrial Aerodynamics 2003; 91(12-15): 1651-1669.

[3] Tang W, Davidson CI, Finger S, Vance K. Erosion of limestone building surfaces caused by wind-driven rain. 1. Field measurements. Atmospheric Environment 2004; 38(33): 5589-5599.

[4] Blocken B, Carmeliet J. A review on wind-driven rain research in building science. Journal of Wind Engineering and Industrial Aerodynamics 2004; 92(13): 1079-1130.

[5] Blocken B, Roels S, Carmeliet J. A combined CFD-HAM approach for wind-driven rain on building facades. Journal of Wind Engineering and Industrial Aerodynamics 2007; 95(7): 585-607.

[6] Janssen H, Blocken B, Carmeliet J. Conservative modelling of the moisture and heat transfer in building components under atmospheric excitation. International Journal of Heat and Mass Transfer 2007; 50(5-6): 1128-1140.

[7] Abuku M, Janssen H, Poesen J, Roels S. Impact, absorption and evaporation of raindrops on building facades. Building and Environment 2009; 44(1): 113-124.

[8] Lacasse MA. IRC studies on the control of rain penetration in exterior wood-frame walls. Solplan Review 2004; 14, January 2004, pp. 14-15.

[9] Bitsuamlak GT, Chowdhury AG, Sambare D. Application of a full-scale testing facility for assessing wind driven rain intrusion. Building and Environment 2009; 44(12): 2430-2441.

[10] Masters FJ, Gurley KR, Prevatt DO. Full-scale simulation of turbulent wind-driven rain effects on fenestration and wall systems. 3rd International Symposium on Wind Effects on Buildings and Urban Environment, March 4-5, 2008, Tokyo, Japan.

[11] Högberg AB, Kragh MK, van Mook FJR. A comparison of driving rain measurements with different gauges. Proc. of the 5th Symp. Build. Phys. in the Nordic Countries, Gothenburg, 24-26 August 1999, 361-368.
[12] van Mook FJR. Driving rain on building envelopes, Ph.D. thesis, Building Physics and Systems, Eindhoven University of Technology, Eindhoven University Press, Eindhoven, The Netherlands, 2002, 198 p.
[13] Blocken B, Carmeliet J. On the accuracy of wind-driven rain measurements on buildings. Building and Environment 2006; 41(12): 1798-1810.
[14] ISO. Hygrothermal performance of buildings – Calculation and presentation of climatic data – Part 3: Calculation of a driving rain index for vertical surfaces from hourly wind and rain data. ISO 15927-3:2009 International Organization for Standardization, 2009.
[15] Straube JF. Moisture control and enclosure wall systems, Ph.D. thesis, Civil Engineering, University of Waterloo, Ontario, Canada, 1998, 318 p.
[16] Straube JF, Burnett EFP. Simplified prediction of driving rain on buildings. Proc. of the International Building Physics Conference, Eindhoven, The Netherlands, 18-21 September 2000, 375-382
[17] Choi ECC. Numerical simulation of wind-driven-rain falling onto a 2-D building. Proceedings of Asia Pacific Conference on Computational Mechanics, Hong Kong, 1991; 1721-1728.
[18] Choi ECC. Simulation of wind-driven rain around a building. Journal of Wind Engineering and Industrial Aerodynamics 1993; 46&47: 721-729.
[19] Choi ECC. Determination of wind-driven rain intensity on building faces. Journal of Wind Engineering and Industrial Aerodynamics 1994; 51: 55-69.
[20] Blocken B, Carmeliet J. Spatial and temporal distribution of driving rain on a low-rise building. Wind and Structures 2002; 5(5): 441-462.
[21] Blocken B, Carmeliet J. On the errors associated with the use of hourly data in wind-driven rain calculations on building facades. Atmospheric Environment 2007; 41(11): 2335-2343.
[22] Hoppestad S. Slagregn i Norge (in Norwegian). Norwegian Building Research Institute, rapport Nr. 13, Oslo, 1955.
[23] Korsgaard V, Madsen TL. Correlation between measured driving rain and computed driving rain. Report of the Heat Insulation Laboratory, Technical University of Denmark, Copenhagen, 1962.
[24] Lacy RE. Driving-rain maps and the onslaught of rain on buildings. RILEM/CIB Symp. on Moisture Problems in Buildings, Rain Penetration, Helsinki, August 16-19, Vol. 3, paper 3-4, 1965.
[25] Lacy RE. Climate and building in Britain. Her Majesty's Stationery Office, London, 1977.
[26] Laws JO, Parsons DA. Relation of raindrop size to intensity. Transactions of the AGU 1943; 24(2): 453-460.
[27] Best AC. Empirical formulae for the terminal velocity of water drops falling through the atmosphere. Quarterly Journal of the Royal Meteorological Society 1950; 76: 302-311.
[28] Blocken B, Carmeliet J. On the validity of the cosine projection in wind-driven rain calculations on buildings. Building and Environment 2006; 41(9): 1182-1189.
[29] Hens H, Ali Mohamed F. Preliminary results on driving rain estimation, Contribution to the IEA annex 24, Task 2—Environmental conditions, T2-B-94/02, 1994.
[30] Flori JP. Influence des conditions climatiques sur le mouillage et le sechage d'une facade verticale (in French), Cahiers du CSTB, livraison 332, September 1992, cahier 2606.
[31] BSI. Methods for assessing exposure to wind-driven rain. Draft for Development 93. British Standards Institution, 1984
[32] BSI. Code of practice for assessing exposure of walls to wind-driven rain – BS8104. British Standards Institution, 1992.
[33] CEN. Hygrothermal performance of buildings – Climatic data – Part 3: Calculation of a driving rain index for vertical surfaces from hourly wind and rain data. Draft prEN 13013-3, 1997.
[34] CEN. Hygrothermal performance of buildings - Calculation and presentation of climatic data - Part 3: Calculation of a driving rain index for vertical surfaces from hourly wind and rain data (ISO/DIS 15927-3:2006). DRAFT prEN ISO 15927-3, 2006.
[35] Blocken B, Carmeliet J. Guidelines for the required time resolution of meteorological input data for wind-driven rain calculations on buildings. Journal of Wind Engineering and Industrial Aerodynamics 2008; 96(5): 621-639.
[36] Best AC. The size distribution of raindrops. Quarterly Journal of the Royal Meteorological Society 1950; 76: 16-36.
[37] Blocken B, Dezsö G, van Beeck J, Carmeliet J. The mutual influence of two buildings on their wind-driven rain exposure and comments on the obstruction factor. Journal of Wind Engineering and Industrial Aerodynamics 2009. In press. doi:10.1016/j.jweia.2009.06.003
[38] Dingle AN, Lee Y. Terminal fall speeds of raindrops. Journal of Applied Meteorology 1972; 11: 877-879.

[39] Choi ECC. Characteristics of the co-occurrence of wind and rain and the driving-rain index. Journal of Wind Engineering and Industrial Aerodynamics 1994; 53: 49-62.
[40] Straube JF, Burnett EFP. Driving rain and masonry veneer, ASTM Symposium on Water Leakage Through Building Facades, Orlando, March 17 1996, Special Technical Publication, ASTM STP 1314, Philadelphia, 1997, pp. 73–87.
[41] Sandberg PI. Driving rain distribution over an infinitely long high building: computerized Calculations. 2nd Int. CIB/RILEM Symp. on Moisture Problems in Buildings. Rotterdam, The Netherlands, 10–12 September 1974, Paper 1-1-2, 1974.
[42] Rodgers GG, Poots G, Page JK, Pickering WM. Theoretical predictions of rain drop impaction on a slab type building. Building Science 1974; 9: 181–190.
[43] Beijer O. Concrete walls and weathering. RILEM/ASTM/CIB Symp. on Evaluation of the Performance of External Vertical Surfaces of Buildings, vol. 1, Otaniemi, Espoo, Finland, August 28–31 and September 1–2, 1977, pp. 67–76.
[44] Rodgers GG. Theoretical studies of the interaction of wind flow with precipitation elements in determining the deposition of rain, snow and ice on buildings and structures. Sixth Course Airflow and Building Design, Sheffield University, 1977.
[45] Hilaire J, Savina H. Pluie battante sur une facade d'immeuble (in French), EN-CLI 88.5 R, CSTB, Nantes, 1988.
[46] Souster C. A theoretical approach to predicting snow loads and driving rain deposition on buildings, Ph.D. Thesis, University of Sheffield, UK, 1979.
[47] Choi ECC. Wind-driven rain on building faces and the driving-rain index. Journal of Wind Engineering and Industrial Aerodynamics 1999; 79: 105-122.
[48] Choi ECC. Variation of wind-driven rain intensity with building orientation. Journal of Architectural Engineering 2000; 6(4): 122-128.
[49] Hangan H. Wind-driven rain studies. A C-FD-E approach. Journal of Wind Engineering and Industrial Aerodynamics 1999; 81: 323-331.
[50] Blocken B, Carmeliet J. The influence of the wind-blocking effect by a building on its wind-driven rain exposure. Journal of Wind Engineering and Industrial Aerodynamics 2006; 94(2): 101-127.
[51] Blocken B, Carmeliet J. Validation of CFD simulations of wind-driven rain on a low-rise building facade. Building and Environment 2007; 42(7): 2530–2548.
[52] Tang W, Davidson CI. Erosion of limestone building surfaces caused by wind-driven rain. 2. Numerical modelling. Atmospheric Environment 2004; 38(33): 5601-5609.
[53] Abuku M, Blocken B, Nore K, Thue JV, Carmeliet J, Roels S. On the validity of numerical wind-driven rain simulation on a rectangular low-rise building under various oblique winds. Building and Environment 2009; 44(3): 621– 632.
[54] Briggen PM, Blocken B, Schellen HL. Wind-driven rain on the facade of a monumental tower: numerical simulation, full-scale validation and sensitivity analysis. Building and Environment 2009; 44(8), 1675–1690.
[55] Choi ECC. Modeling of wind-driven rain and its soil detachment effect on hill slopes. Journal of Wind Engineering and Industrial Aerodynamics 2002; 90: 1081-1097.
[56] Blocken B, Carmeliet J, Poesen J. Numerical simulation of the wind-driven rainfall distribution over small-scale topography in space and time. Journal of Hydrology 2005; 315(1-4): 252-273.
[57] Blocken B, Poesen J, Carmeliet J. Impact of wind on the spatial distribution of rain over micro-scale topography – numerical modelling and experimental verification. Hydrological Processes 2006; 20(2): 345-368.
[58] Karagiozis A, Hadjisophocleous G, Cao S. Wind-driven rain distributions on two buildings. Journal of Wind Engineering and Industrial Aerodynamics 1997; 67&68: 559-572.
[59] Melese Endalew A, Hertog M, Delele MA, Baetens K, Persoons T, Baelmans M, Ramon, H, Nicolai BM, Verboven P. CFD modelling and wind tunnel validation of airflow through plant canopies using 3D canopy architecture. International Journal of Heat and Fluid Flow 2009; 30(2): 356-368.
[60] Melese Endalew A, Hertog M, Gebreslasie Gebrehiwot M, Baelmans M, Ramon H, Nicolai BM, Verboven P. Modelling airflow within model plant canopies using an integrated approach. Computers and Electronics in Agriculture 2009; 66(1): 9-24.
[61] Richards PJ, Hoxey RP. Appropriate boundary conditions for computational wind engineering models using the k-ε turbulence model. Journal of Wind Engineering and Industrial Aerodynamics 1993; 46&47: 145-153.
[62] Blocken B, Stathopoulos T, Carmeliet J. CFD simulation of the atmospheric boundary layer: wall function problems. Atmospheric Environment 2007; 41(2): 238-252.

[63] Blocken B, Carmeliet J, Stathopoulos T. CFD evaluation of the wind speed conditions in passages between buildings – effect of wall-function roughness modifications on the atmospheric boundary layer flow. Journal of Wind Engineering and Industrial Aerodynamics 2007; 95(9-11): 941-962.
[64] Franke J, Hellsten A, Schlünzen H, Carissimo B. Best practice guideline for the CFD simulation of flows in the urban environment. COST Action 732: Quality Assurance and Improvement of Microscale Meteorological Models, 2007.
[65] Gorlé C, van Beeck J, Rambaud P, Van Tendeloo G. CFD modelling of small particle dispersion: the influence of the turbulence kinetic energy in the atmospheric boundary layer. Atmospheric Environment 2009; 43(3) 673-681.
[66] Choi ECC. Numerical modeling of gust effect on wind-driven rain. Journal of Wind Engineering and Industrial Aerodynamics 1997; 72: 107-116.
[67] Janssen H, Blocken B, Roels S, Carmeliet J. Wind-driven rain as a boundary condition for HAM simulations: analysis of simplified modelling approaches. Building and Environment 2007; 42(4): 1555-1567.
[68] Loth E. Numerical approaches for motion of dispersed particles, droplets, and bubbles. Progress in Energy and Combustion Science 2000; 26: 161–223.
[69] Shirolkar JS, Coimbra CFM, McQuay MQ. Fundamental aspects of modeling turbulent particle dispersion in dilute flows. Progress in Energy and Combustion Science 1996; 22(4): 363–399.
[70] Zhang Z, Chen Q. Comparison of the Eulerian and Lagrangian methods for predicting particle transport in enclosed spaces. Atmospheric Environment 41(25): 5236-5248.

Description of wall	Average value	Distribution
Two-storey gable	0,4	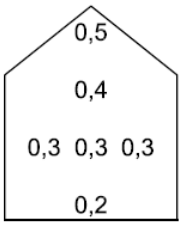
Three-storey gable	0,3	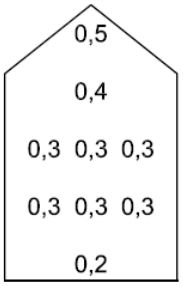
Multi-storey building with flat roof (pitch < 20°)	0,2 for a ten-storey building, for example, but with a higher intensity at top	0,5 for top 2,5 m 0,2 for remainder
Two-storey wall with eaves	0,3	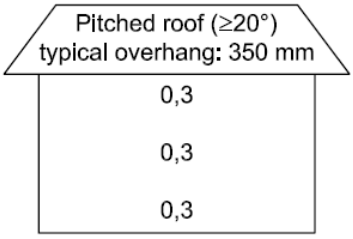
Three-storey wall with eaves	0,4	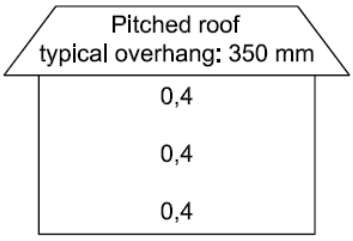
Two-storey building with flat roof (pitch < 20°)	0,4	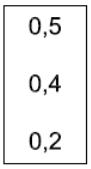

Fig. 1. Wall factors (W) in the 2009 ISO Standard (© ISO 2009, reproduced with permission).

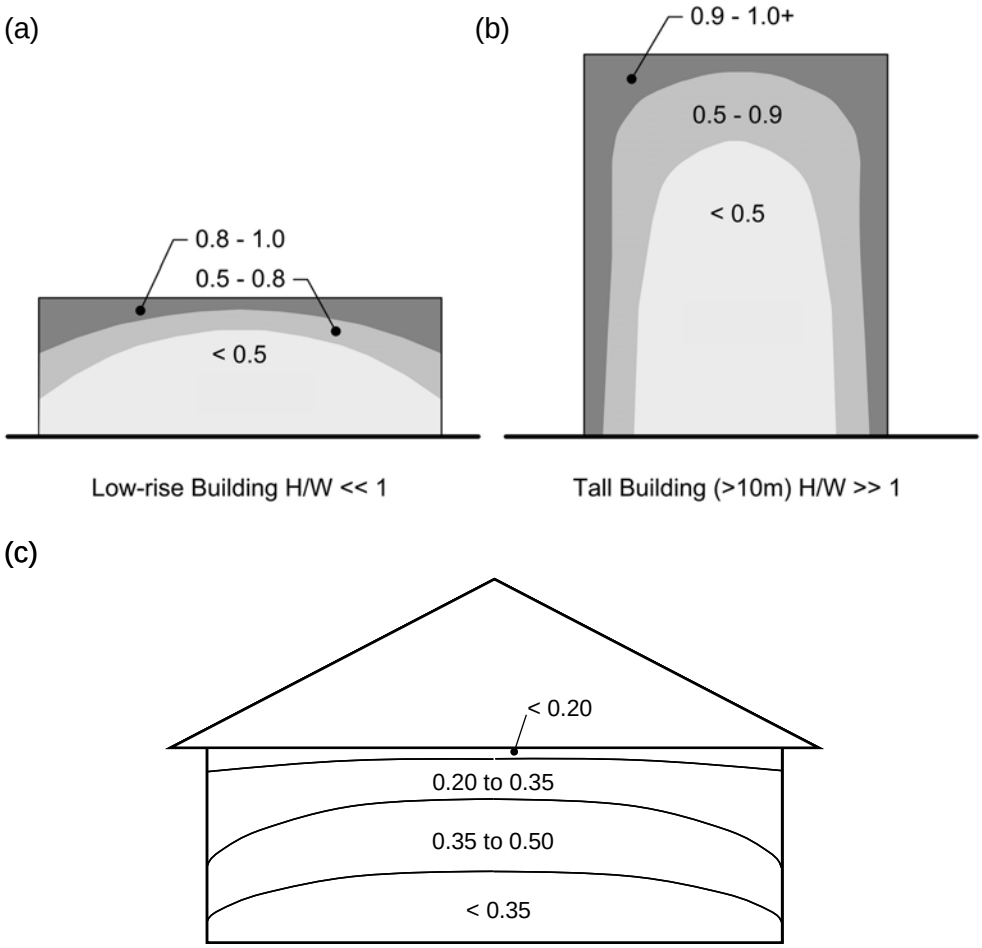

Fig. 2. Rain admittance factors (RAF) as provided by Straube [15] and Straube and Burnett [16]: (a) Low-rise building with H/W << 1; (b) Tall building (> 10 m) with H/W >> 1; (c) Low-rise building with sloped roof and roof overhang.

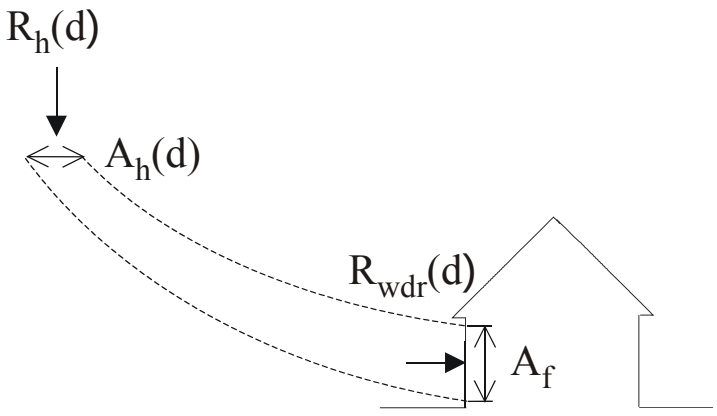

Fig. 3. Method to determine the specific catch ratio in the CFD model by Choi. Stream tube bounded by two trajectories of raindrops with diameter d. The specific catch ratio η_d for zone A_f and for raindrops with diameter d is determined based on conservation of mass for the raindrops in the stream tube.

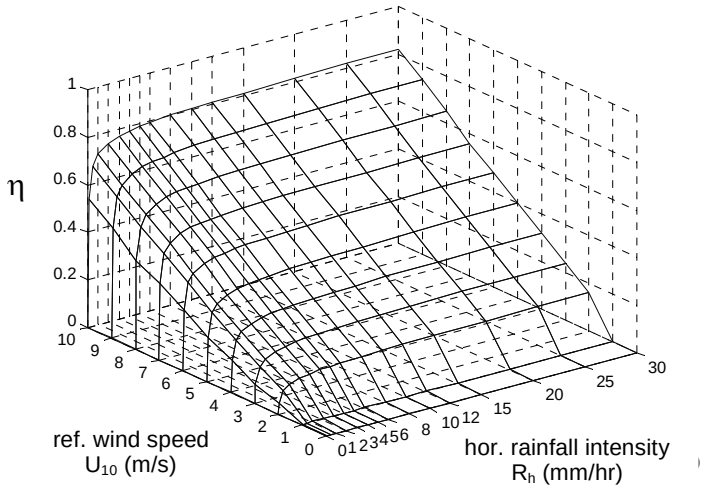

Fig. 4. Typical example of a catch-ratio chart or η-chart that presents the catch ratio η as a function of reference wind speed U_{10} and horizontal rainfall intensity R_h, for a given position on the building facade and for a given wind direction [50].

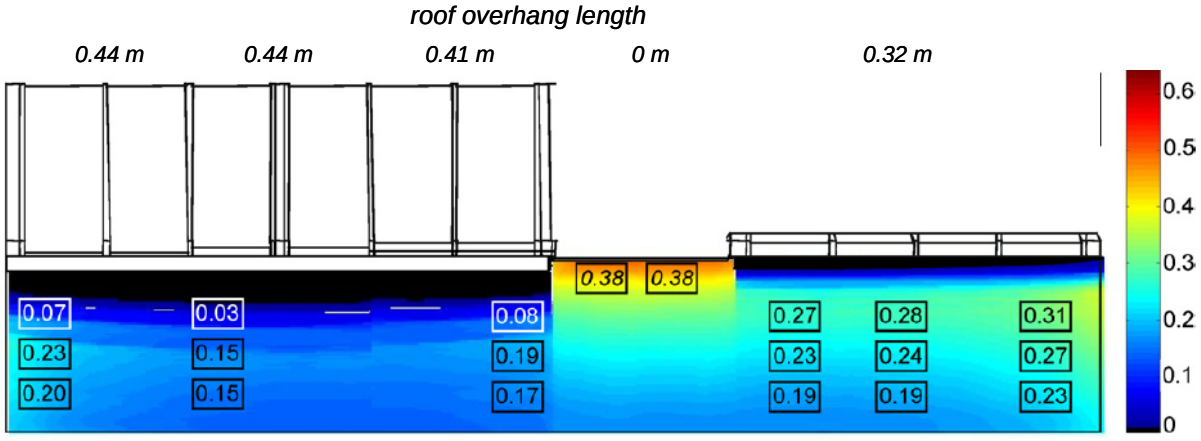

Fig. 5. CFD results for distribution of the ratio S_{wdr}/S_h (accumulated wind-driven rain to accumulated horizontal rainfall) across the south-west facade of the VLIET test building at the end of a rain event [51]. Black areas indicate regions sheltered from rain by roof overhang.

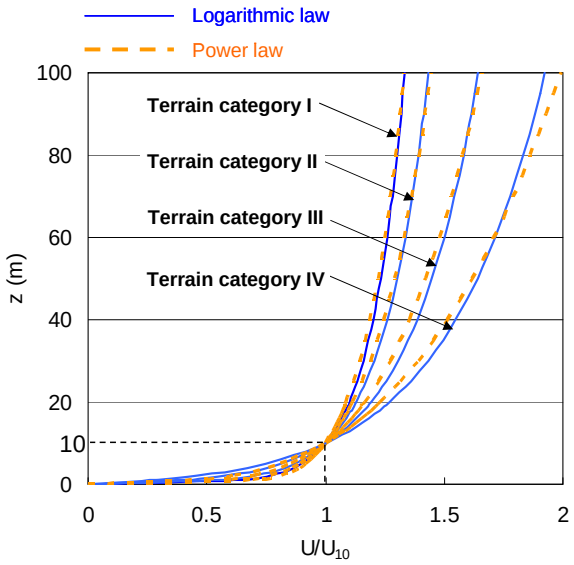

Fig. 6. Fit of power law and logarithmic law for the four terrain categories in the ISO Standard (see Table 1). The profiles are matched at 10 m height.

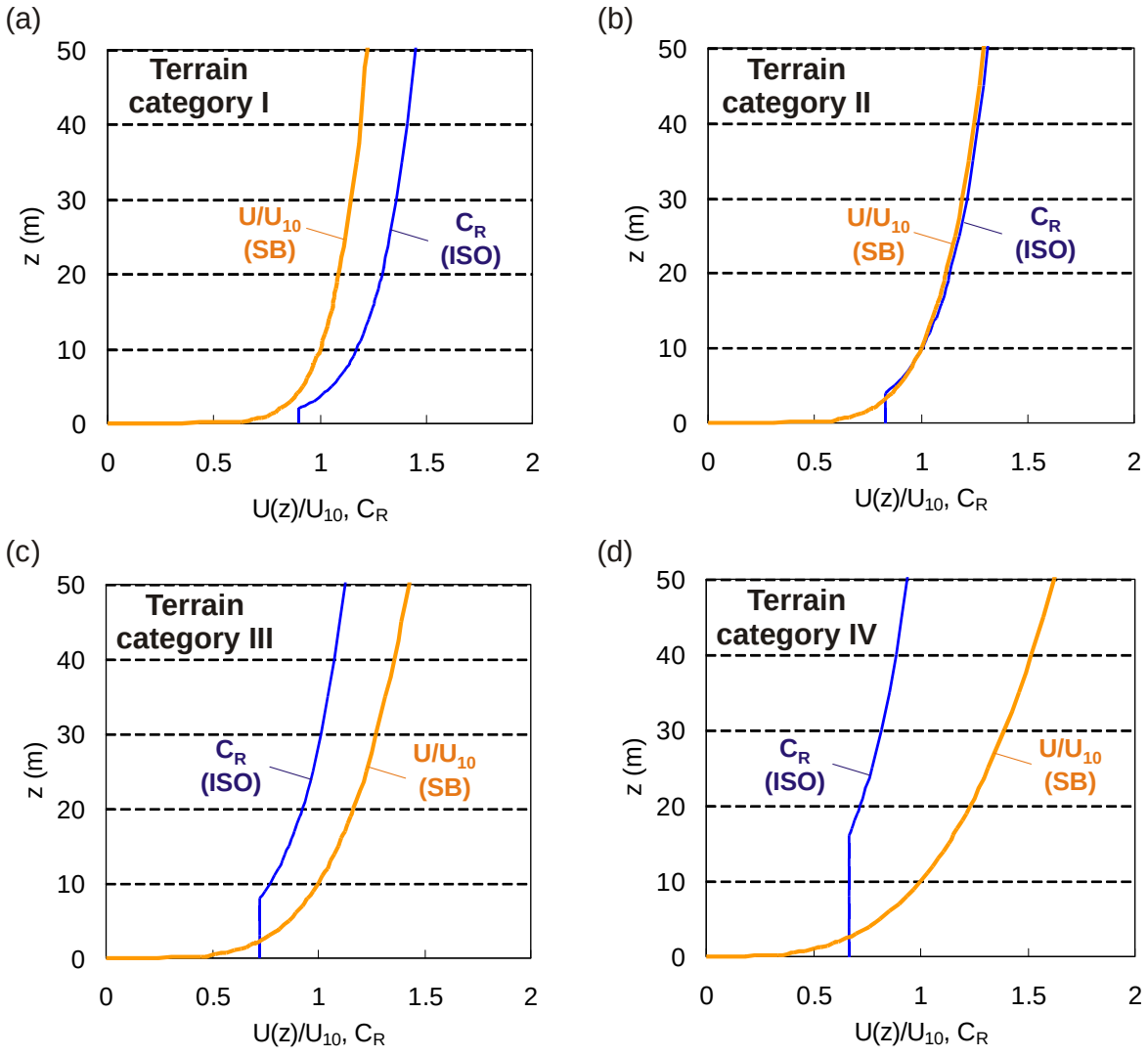

Fig. 7. Comparison of implementation of terrain roughness and variation of wind speed with height in the ISO Standard (ISO) and in the model by Straube and Burnett (SB).

Table 1. Parameters in the ISO Standard roughness coefficient [14]

Terrain category	Description	K_R	z_0	z_{min}
I	Rough open sea; lake shore with at least 5 km open water upwind and smooth flat country without obstacles	0.17	0.01	2
II	Farm land with boundary hedges, occasional small farm structures, houses or trees	0.19	0.05	4
III	Suburban or industrial areas and permanent forests	0.22	0.3	8
IV	Urban areas in which at least 15% of the surface is covered with buildings of average height exceeding 15 m	0.24	1	16

Table 2. ISO Standard obstruction factor as a function of the distance of the obstruction from the facade [14].

Distance of obstruction from facade (m)	Obstruction factor O
4 - 8	0.2
8 - 15	0.3
15 - 25	0.4
25 - 40	0.5
40 - 60	0.6
60 - 80	0.7
80 - 100	0.8
100 - 120	0.9
over 120	1.0

Table 3. Comparison of models in terms of implementation of influencing parameters of wind-driven rain.

Parameter	**ISO Standard (ISO)**	**Straube and Burnett (SB)**	**CFD model (CFD)**
1. Building geometry	5 types of low-rise buildings 1 type of high-rise building	3 types of buildings and "building-scale independence"	All possible geometries
2. Position on facade	Wall factor: average values at discrete positions (Fig. 1)	RAF: constant interval regions (Fig. 2)	High resolution, defined by user
3. Environment topography			
3.1. Roughness of terrain	Roughness coefficient C_R (log law)	Power law exponent β	Included (inlet profiles and ground-roughness specification)
3.2. Hills, cliffs, valleys	Topography coefficient C_T	-	Can be included in detail
3.3. Surrounding buildings	Obstruction factor O	-	Can be included in detail
3.4. Surrounding trees	Obstruction factor O	-	Can be included in detail
4. Wind speed			
4.1. Mean wind speed			
4.1.1. Variation with height	Roughness coefficient C_R (log law)	Power law exponent β	Included (inlet profiles)
4.1.2. Flow around building	Wall factor: time-averaged values	RAF: time-averaged values	Included
4.2. Turbulent dispersion	Implicitly in wall factor W (based on measurements)	Implicitly in RAF (based on measurements)	Can be included in detail
5. Wind direction	Cosine projection	Cosine projection	Can be included in detail
6. Hor. rainfall intensity	Only in model eq. (5,6,11)	In DRF (eq. 12-15) In model eq. (16)	In model eq. (19) Fully included
7. Raindrop-size distribution	Implicitly in wall factor W (based on measurements)	Implicitly in RAF Mean diameter of assumed distribution in DRF (eq. 12-15)	Assumed distribution Complete distribution is taken into account